J Mater Sci (2008) 43:6223–6232
DOI 10.1007/s10853-008-2920-7

Analytical modeling of residual stresses in multilayered superconductor systems

C. H. Hsueh · M. Paranthaman

Received: 2 June 2008 / Accepted: 31 July 2008 / Published online: 26 August 2008

Abstract Residual stresses-induced damages in multilayered films grown on technical substrates present a reliability issue for the fabrication and applications of multilayered superconductor systems. Using closed-form solutions for residual stresses in multilayered systems, specific results were calculated for residual stresses induced by the lattice and the thermal mismatches in the system of YBCO/CeO_2/YSZ/Y_2O_3 films on a Ni-5 W substrate. It was concluded that lattice mismatch-induced residual stresses must be relaxed by forming interfacial defects. Studies of residual thermal stresses showed the following. When the thickness of a film is negligible compared to the substrate, the changes of its properties modify the residual stresses in this film layer but have negligible effects on the residual stresses in other layers in the system. On the other hand, when the thickness of certain film layer is not negligible compared to the substrate, residual stresses in each layer can be controlled by adjusting the properties and thickness of this film layer. Finally, the effects of buffer layers on thermal stresses in $YBa_2Cu_3O_{7-x}$ (YBCO) were addressed by using YBCO/$LaMnO_3$/homo-epi MgO/IBAD MgO/Y_2O_3/Al_2O_3 films on Hastelloy substrate as an example.

C. H. Hsueh (✉)
Materials Science and Technology Division, Oak Ridge National Laboratory, Oak Ridge, TN 37831, USA
e-mail: hsuehc@ornl.gov

M. Paranthaman
Chemical Sciences Division, Oak Ridge National Laboratory, Oak Ridge, TN 37831, USA

Introduction

$YBa_2Cu_3O_{7-x}$ (YBCO) coated conductors have potential applications for electric power and superconducting magnet technologies. The major criteria for fabricating high performance superconducting wires are: ability to carry high critical current at high magnetic fields, high mechanical strength, stability, cost effectiveness, and long length. The second generation YBCO coated conductors have been developed by using three major approaches [1]: rolling-assisted biaxially textured substrate (RABiTS) process, ion-beam-assisted deposition (IBAD), and inclined substrate deposition (ISD). Among these three approaches, RABiTS and IBAD are more promising in terms of low manufacture cost, flexibility, and high critical current density for high temperature superconductor applications. The most commonly used RABiTS architectures consist of a starting template of biaxially textured Ni-5 at.% W substrate with a seed layer of Y_2O_3, a barrier layer of YSZ, and a CeO_2 cap layer [2]. These three buffer layers are generally deposited using physical vapor deposition (PVD) techniques, and the purpose of buffer layers is to (i) provide a smooth and chemically inert surface for the growth of the YBCO film while transferring the biaxial texture from the substrate to YBCO, (ii) prevent metal diffusion from the substrate into YBCO, (iii) act as oxygen diffusion barrier to avoid substrate oxidation, and (iv) provide mechanical stability and good adhesion to the substrate [3]. On top of the PVD template, YBCO film is then grown by metal-organic deposition. However, pulsed laser deposition has also been frequently used to grow YBCO films for testing various buffer layers.

In a multilayered system, the existence of residual stresses is inevitable which can result in cracking and/or delamination of film layers. To improve the reliability of

multilayered superconductor systems, understanding of the issue of residual stresses is essential which can result from the lattice and the thermal mismatches between the constituent layers. When the layer arrangement is asymmetric in the thickness direction, the residual stress distribution through the thickness of the system is also asymmetric which, in turn, results in bending of the system. Residual stresses and bending in layered systems were first analyzed by Stoney [4], in which a bilayered strip consisting of a film and a substrate was considered, and a simple equation was derived to relate the stress in the film to the curvature of the system. However, Stoney's equation is valid only when the film thickness is infinitesimal compared to the substrate thickness. The general solution for residual stresses in bilayered systems was first derived by Timoshenko [5], in which a bilayered strip subjected to a temperature change was considered. The analysis was based on classical beam theory and started by assuming the individual force and bending moment in each layer. The bending moment was related to the curvature of the layer, and both layers were assumed to have the same curvature. Then, by balancing the forces and moments in the system and by including the temperature-induced, force-induced, and bending-induced strains to satisfy the strain continuity condition at the interface between the two layers, the solution was obtained. Timoshenko's approach has been adopted by many others to analyze the thermal stresses in multilayered systems [6–10]. However, for a multilayered system, both the number of unknowns to be solved and the number of continuity conditions to be satisfied at the interfaces increase with the number of layers [6–10]. As a result, the degree of difficulties in solving the residual stresses increases with the number of layers in the system. Alternatively, the multilayer problem can be solved using laminate theory [11]. However, its solutions are often expressed in matrices, and computers are used to obtain the numerical results.

A simple analytical model for analyzing residual stresses in multilayered systems has been developed recently [12, 13], the closed-form solutions are exact for locations remote from the free edges of the system, and the accuracy of solutions has been verified by finite element results [14]. The essence of this model is to decompose the strain through the thickness of the multilayered system into a uniform and bending components, and the continuity conditions at the interfaces are automatically satisfied. There are only three unknowns to be solved and three boundary conditions to be satisfied regardless of the number of layers in the system, and simple closed-form solutions for residual stresses can hence be obtained by balancing forces and moments in the system. The purpose of the present study was to apply the closed-form solutions [12, 13] to analyze the residual stresses in multilayered superconductor systems. Other different formulations of the closed-form solutions can also be found elsewhere [15, 16]. First, the analytical model and the closed-form solutions for residual stresses in multilayered systems were summarized. Then, specific results were calculated for YBCO/CeO_2/YSZ/Y_2O_3/Ni-5 W five-layered superconductor systems. Residual stresses resulting from the lattice and the thermal mismatches were analyzed, respectively. The effects of (i) the thickness of YBCO film layer, (ii) the thickness of Ni-5 W substrate, and (iii) replacing YSZ layer with $La_2Zr_2O_7$ layer on the thermal stress distribution through the thickness of the multilayered system were examined. Finally, the effects of buffer layers on thermal stresses in YBCO were addressed by using YBCO/$LaMnO_3$/MgO/MgO/Y_2O_3/Al_2O_3/Hastelloy seven-layered IBAD system as an example.

Summary of analytical model

Modeling for residual stresses induced by the thermal mismatch was summarized here, and the results could be extended to the case of lattice mismatch. The cross section of a multilayered system is shown schematically in Fig. 1, where n film layers with individual thicknesses, t_i, are bonded sequentially to a substrate with a thickness, t_s, at elevated temperatures. The subscript, i, denotes the layer number and ranges from 1 to n with layer 1 being the one in direct contact with the substrate. The coordinate system is defined such that the layer 1/substrate interface is located at $z = 0$, the free surfaces of the substrate and layer n are located at $z = -t_s$ and $z = h_n$, respectively, and the interface between layers i and $i + 1$ is located at $z = h_i$. With these definitions, the relation between h_i and t_i is described by

$$h_i = \sum_{j=1}^{i} t_j \quad (i = 1 \text{ to } n). \tag{1}$$

The multilayered system is subjected to a temperature change, ΔT, from a stress-free temperature and the

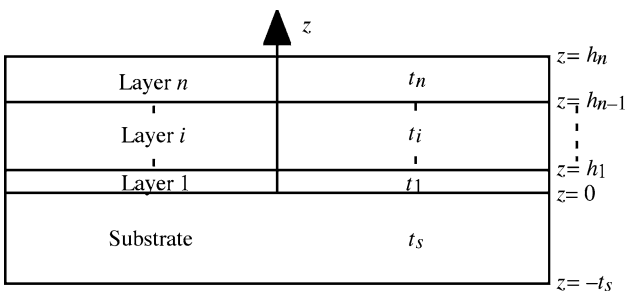

Fig. 1 Schematic showing the cross section of multilayered system and the coordinate system used in the analysis

coefficients of thermal expansion (CTEs) of the substrate and films are α_s and α_i, respectively. Due to the asymmetric layer arrangement, the thermal mismatch between layers results in bending of the multilayered system. At positions away from the edges of the system, the stresses induced by the thermal mismatch are in-plane (i.e., parallel to the interface) and (equi)biaxial for the planar geometry, and both the stress normal to the interface and the interfacial shear stress are zero.

General solutions

By decomposing the total strain in the system into a uniform and a bending components, the in-plane biaxial stress distributions in the substrate and film layers, σ_s and σ_i, can be expressed as [12, 13]

$$\sigma_s = E'_s\left(c + \frac{z-b}{r} - \alpha_s\Delta T\right) \quad (\text{for } -t_s \le z \le 0), \tag{2a}$$

$$\sigma_i = E'_i\left(c + \frac{z-b}{r} - \alpha_i\Delta T\right) \quad (\text{for } i = 1 \text{ to } n), \tag{2b}$$

where $E' = E/(1-\nu)$ is the biaxial modulus, E and ν are Young's modulus and Poisson's ratio, respectively, c is the uniform strain component, $z = b$ denotes the position of the bending axis at which the bending strain component is zero, and r is the radius of curvature of the multilayered system.

The three parameters, c, b, and r, can be derived sequentially by satisfying the following three boundary conditions: (i) the resultant force due to the uniform strain component is zero, (ii) the resultant force due to the bending strain component is zero, and (iii) the resultant bending moment due to the stresses described by Eqs. 2a and 2b is zero. These three boundary conditions are described, respectively, by

$$E'_s(c - \alpha_s\Delta T)t_s + \sum_{i=1}^{n} E'_i(c - \alpha_i\Delta T)t_i = 0 \tag{3a}$$

$$\int_{-t_s}^{0} \frac{E'_s(z-b)}{r}dz + \sum_{i=1}^{n}\int_{h_{i-1}}^{h_i} \frac{E'_i(z-b)}{r}dz = 0 \tag{3b}$$

$$\int_{-t_s}^{0} \sigma_s z dz + \sum_{i=1}^{n}\int_{h_{i-1}}^{h_i} \sigma_i z dz = 0 \tag{3c}$$

When $i = 1$, h_{i-1} (i.e., h_0) in Eqs. 3b and 3c is defined as zero.

With the above three boundary conditions, the solutions of the three parameters can be obtained, such that

$$c = \frac{\left(E'_s t_s\alpha_s + \sum_{i=1}^{n} E'_i t_i\alpha_i\right)\Delta T}{E'_s t_s + \sum_{i=1}^{n} E'_i t_i}, \tag{4a}$$

$$b = \frac{-E'_s t_s^2 + \sum_{i=1}^{n} E'_i t_i(2h_{i-1} + t_i)}{2\left(E'_s t_s + \sum_{i=1}^{n} E'_i t_i\right)}, \tag{4b}$$

$$\frac{1}{r} = \frac{3\left[E'_s(c - \alpha_s\Delta T)t_s^2 - \sum_{i=1}^{n} E'_i t_i(c - \alpha_i\Delta T)(2h_{i-1} + t_i)\right]}{E'_s t_s^2(2t_s + 3b) + \sum_{i=1}^{n} E'_i t_i\left[6h_{i-1}^2 + 6h_{i-1}t_i + 2t_i^2 - 3b(2h_{i-1} + t_i)\right]}. \tag{4c}$$

With the solutions of c, b, and r, the general solutions for the stress distributions in multilayered systems are complete. Both σ_s in the substrate and σ_i in each film layer given by Eqs. 2a and 2b are functions of z. The above solutions are exact for positions in the multilayered system remote from the free edges. In the presence of the temperature dependence of CTE, the thermal strain $\alpha\Delta T$ should be replaced by an integral of the CTE with respect to the temperature. Alternatively, this thermal strain can also be expressed by $\alpha^*\Delta T$ where α^* is the average CTE within the temperature range. Also, the above solutions can be used to analyze the residual stresses induced by the lattice mismatch. In this case, the thermal strain in the substrate, $\alpha_s\Delta T$, is replaced by zero and the thermal strains in the film layers, $\alpha_i\Delta T$, are replaced by the lattice mismatch strains of the films with respect to the substrate, $\Delta\varepsilon_i$.

Thin film approximations

It should be noted that no constraints are imposed on the relation between the film thickness and the substrate thickness for the above general solutions, and the film and the substrate can have comparable thicknesses. Although the general solutions given in the Section "General solutions" are closed-form, the functional dependences of the stresses on material properties and thickness of each layer

cannot be readily seen. Hence, thin film approximations are considered in this section.

When the films are thin compared to the substrate, the above exact solutions can be simplified, such that the solutions from the first order approximation are [12, 13]

$$\sigma_s = \frac{2}{t_s^2}\left(3z + 2t_s - \frac{2}{E_s'}\sum_{j=1}^{n} E_j' t_j\right)\sum_{i=1}^{n} E_i' t_i(\alpha_i - \alpha_s)\Delta T \quad (\text{for } -t_s \le z \le 0), \tag{5a}$$

$$\sigma_i = E_i'\left(\alpha_s - \alpha_i + 4\sum_{j=1}^{n}\frac{E_j' t_j(\alpha_j - \alpha_s)}{E_s' t_s}\right)\Delta T \quad (\text{for } i = 1 \text{ to } n). \tag{5b}$$

When the film thicknesses are negligible, Eqs. 5a and 5b can be further simplified, such that the solutions from the zero order approximation are

$$\sigma_s = \frac{2}{t_s^2}(3z + 2t_s)\sum_{i=1}^{n} E_i' t_i(\alpha_i - \alpha_s)\Delta T \quad (\text{for } -t_s \le z \le 0), \tag{6a}$$

$$\sigma_i = E_i'(\alpha_s - \alpha_i)\Delta T \quad (\text{for } i = 1 \text{ to } n). \tag{6b}$$

With the stresses given by simple equations, Eqs. 5a, 5b and 6a, 6b, some special features can be observed for thin film approximations. (i) It can be seen from Eqs. 5a and 6a that the magnitude of thermal stress in the substrate, σ_s, is relatively small when the films are thin. (ii) The location of the neutral axis is located at two-thirds of the substrate thickness underneath the film/substrate interface; i.e., $\sigma_s = 0$ at $z = -2t_s/3$ in Eq. 6a, when $t_s \gg t_i$. The neutral axis shifts away from $z = -2t_s/3$ when the film thickness is not negligible, and this shift is dictated by the third term in the parenthesis in Eq. 5a. (iii) Based on Eqs. 5b and 6b, the variation of thermal stresses through the thickness of each thin film layer can be ignored (i.e., σ_i is independent of z). (iv) The thermal stress in each thin film layer is controlled by the mismatch between the individual film layer and the substrate (see Eq. 6b) and is insensitive of the presence of other film layers while the sensitivity is dictated by the third term in the parenthesis in Eq. 5b.

Results

Specific results were calculated using the exact solutions, Eqs. 2a, 2b and 4a–c, for 1–3 μm YBCO/75 nm CeO_2/75 nm YSZ/75 nm Y_2O_3/50–75 μm Ni-5 W five-layered superconductor system that is schematically shown in Fig. 2. When the film is sufficiently thin, the special features discussed in the Section "Thin film approximations" for thin film approximations should be reflected from the results obtained from the general exact solutions shown in Section "General solutions". The thermomechanical properties of the constituent layers and the lattice mismatch strains of films with respect to the Ni-5 W substrate are listed in Table 1 (M. Paranthaman, Private communication) [17–21]. Unless noted otherwise, 1-μm thick YBCO and 50-μm thick Ni-5 W were used in calculations.

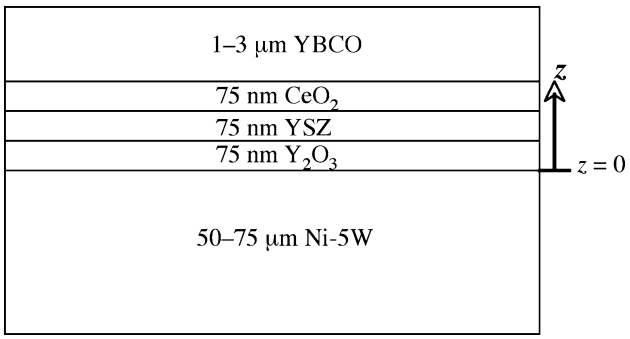

Fig. 2 Schematic showing the layer arrangement and dimensions of the multilayered superconductor system consisting of YBCO/CeO_2/YSZ/Y_2O_3 film layers on Ni-5 W substrate

Stresses due to lattice mismatch

Assuming perfect epitaxial growth for all films without any form of stress relaxation, the calculated elastic stresses in the films and the substrate are shown, respectively, in Fig. 3a and b. The horizontal dashed lines in Fig. 3a correspond to the locations of interfaces between film layers. The positive and negative signs of stresses indicate tensile and compressive stresses, respectively. While all the film layers are subjected to compression, the substrate is subjected to combined tension/compression because of bending that results from the asymmetric stress distribution through the thickness of the system. However, because the substrate has the smallest lattice parameter in the system, net tension exists in the substrate. Based on the predicted elastic stresses, the system is unable to withstand such high stresses that can induce macroscopic cracks such as tunnel cracks or delaminations [22]. However, these macroscopic cracks have not been observed during the film growth processes. Hence, the lattice mismatch-induced stresses are presumably relaxed by lattice distortion, tilting of the lattice plane, or forming interfacial misfit dislocations/stacking faults during the film growth processes [23–29]. It should be noted that by comparing the residual stresses measured by X-ray diffraction with the calculated thermal stresses, it has been concluded that stresses due to lattice mismatch are not fully relaxed [17, 30]. These un-relaxed stresses would superpose on thermal stresses to give the resultant residual stresses. Furthermore, when energetic particle bombardment is involved in film deposition, it would induce additional compressive stresses in the film [17, 30].

Table 1 Thickness and materials properties of the constituent layers in YBCO/CeO_2/YSZ/Y_2O_3/Ni-5 W five-layered RABiTS-based superconductor system

Materials	Thickness	Young's modulus (GPa)	Poisson's ratio	CTE × 10^{-6}/°C	% Lattice mismatch versus Ni-5 W
YBCO	1–3 μm	157 [17]	0.3 [17]	12 (M. Paranthaman, Private communication)	8.1 [3]
CeO_2	75 nm	165 [18]	0.3 [18]	11 [18]	8.22 [3]
YSZ	75 nm	140 [19]	0.25 [18]	9.7 [17]	3.07 [3]
Y_2O_3	75 nm	128 [19]	0.3	9.3 [20]	6.22 [3]
Ni-5 W	50–75 μm	118 [21]	0.33	16 (M. Paranthaman, Private communication)	0

All the references are given in square brackets

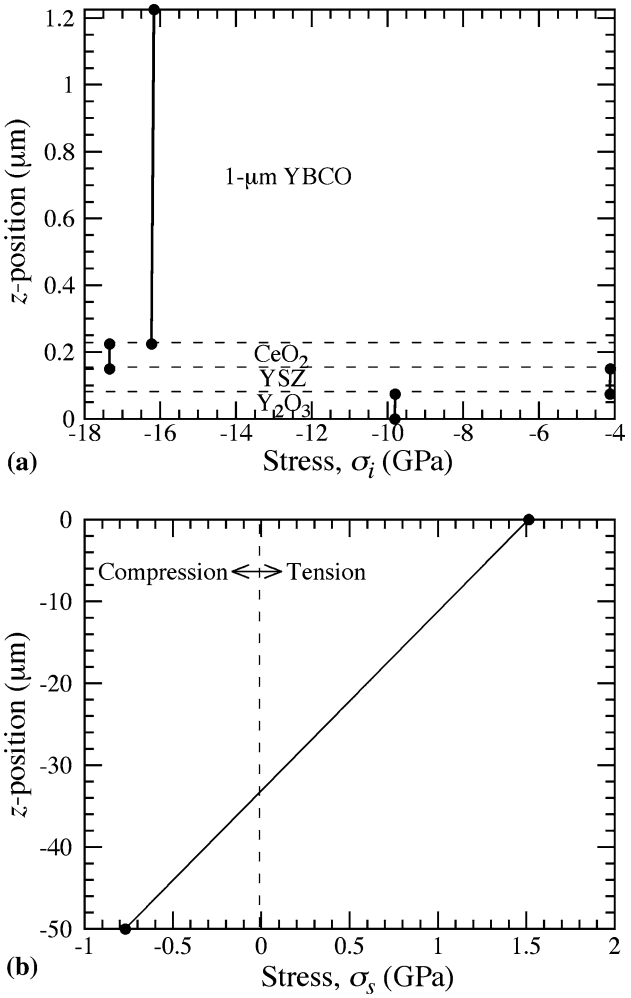

Fig. 3 Lattice mismatch-induced stresses in (**a**) YBCO/CeO_2/YSZ/Y_2O_3 films and (**b**) Ni-5 W substrate

Stresses due to thermal mismatch

Assuming that the system is stress-free at the YBCO growth temperature, 700–800 °C, [3] thermal stresses are calculated based on the temperature change from the stress-free temperature, ~750 °C, to room temperature; i.e., $\Delta T = -725$ °C.

Effects of YBCO thickness

$YBa_2Cu_3O_{7-x}$ is the active layer providing superconductivity. Theoretically, a thick YBCO layer is preferred for high current density. However, cracking of YBCO is promoted upon external bending of the multilayered system with a thick YBCO layer. In practice, YBCO thicknesses of 1–3 μm have been used. To study the effects of YBCO thickness, calculated thermal stresses in the film layers are shown in Fig. 4a, b, and c, respectively, for YBCO thicknesses of 1, 2, and 3 μm. The magnitudes of compressive stresses in all the film layers decrease as the YBCO thickness increases. The corresponding thermal stress in the Ni-5 W substrate is shown in Fig. 4d. The magnitude of stresses in the substrate is relatively small compared to those in films, and both the stress gradient and the magnitude of stresses in the substrate increase as the YBCO thickness increases. This trend of the stress gradient is reflected by the increasing curvature of the system with the YBCO thickness, which is shown in Fig. 5. It can be observed from Fig. 4d that the location of neutral axis (i.e., zero stress) is located at about two-thirds of the substrate thickness underneath the film/substrate interface. While different models can be performed to predict the thermal stress distribution in multilayer, this location of neutral axis serves as a checkpoint for the predicted results when the films are much thinner than the substrate. It should also be noted that if the film thickness is negligible compared to the substrate thickness, the residual stress in each film layer described by Eq. 6b is dictated by the mismatch between the individual film layer and the substrate and is independent of the presence of other film layers. The dependence of the residual stress in each film layer on the thickness of YBCO shown in Fig. 4a, b, and c signifies that the YBCO thickness (1–3 μm) is not negligible compared to the substrate thickness (50 μm). While the stresses in CeO_2,

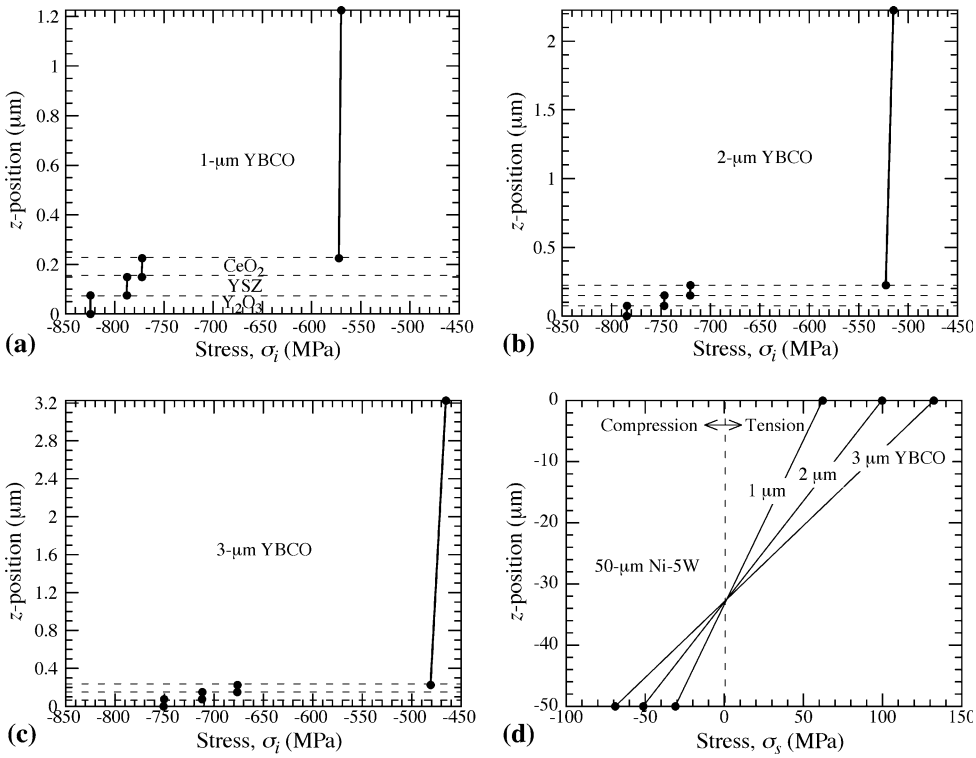

Fig. 4 Thermal stresses in YBCO/CeO_2/YSZ/Y_2O_3 films for YBCO thickness of (**a**) 1 μm, (**b**), 2 μm, and (**c**) 3 μm, and (**d**) thermal stresses in Ni-5 W substrate

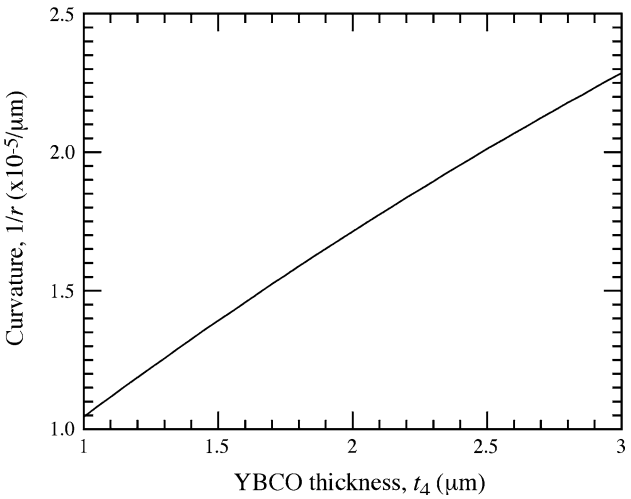

Fig. 5 The curvature of YBCO/CeO_2/YSZ/Y_2O_3/Ni-5 W five-layered systems as a function of YBCO thickness

YSZ, and Y_2O_3 are almost uniform within each layer, the stress in YBCO shows noticeable gradient as its thickness increases from 1 to 3 μm.

Effects of Ni-5 W substrate thickness

The nominal thickness of the multilayered superconductor system with Ag and Cu cap layers is 100–200 μm, and the thickness of Ni-5 W substrate used in the system is generally 50–75 μm. To examine the effects of substrate thickness, calculated thermal stresses in the film layers and the substrate are shown, respectively, in Fig. 6a and b for substrate thicknesses of 50 and 75 μm. YBCO thickness of 2 μm was used in these calculations. When the substrate thickness increases, the magnitudes of compressive stresses in all film layers increase but the stress gradient and the magnitude of stresses in the substrate decrease. Again, the location of neutral axis is located at about two-thirds of the substrate thickness underneath the film/substrate interface for $t_s = 50$ and 75 μm (see Fig. 6b).

Effects of replacing YSZ with $La_2Zr_2O_7$ film layer

The commonly used buffer layers, CeO_2/YSZ/Y_2O_3, grown by PVD are not cost effective. It has been reported that various buffer layers can be grown on textured Ni-alloy substrates using chemical solution deposition, which has the advantages of (i) ease in controlling the composition, (ii) relatively low processing temperature, and (iii) cost effectiveness. Among the various buffer layers, $La_2Zr_2O_7$ has a cubic pyrochlore structure, is stable over 1,500 °C, and has a close lattice mismatch (~0.7%) with YBCO. Therefore, $La_2Zr_2O_7$ is considered to be one of the most suitable buffer layers for the preparation of YBCO coated conductors [31–37]. The properties of $La_2Zr_2O_7$ are [35]: $E = 175$ GPa, $\nu = 0.11$, $\alpha = 7.4 \times 10^{-6}/°C$. Replacing YSZ layer with $La_2Zr_2O_7$, the calculated thermal stresses in the film layers and the substrate are shown in Fig. 7a and b, respectively. Compared to Fig. 4a and d, the replacement

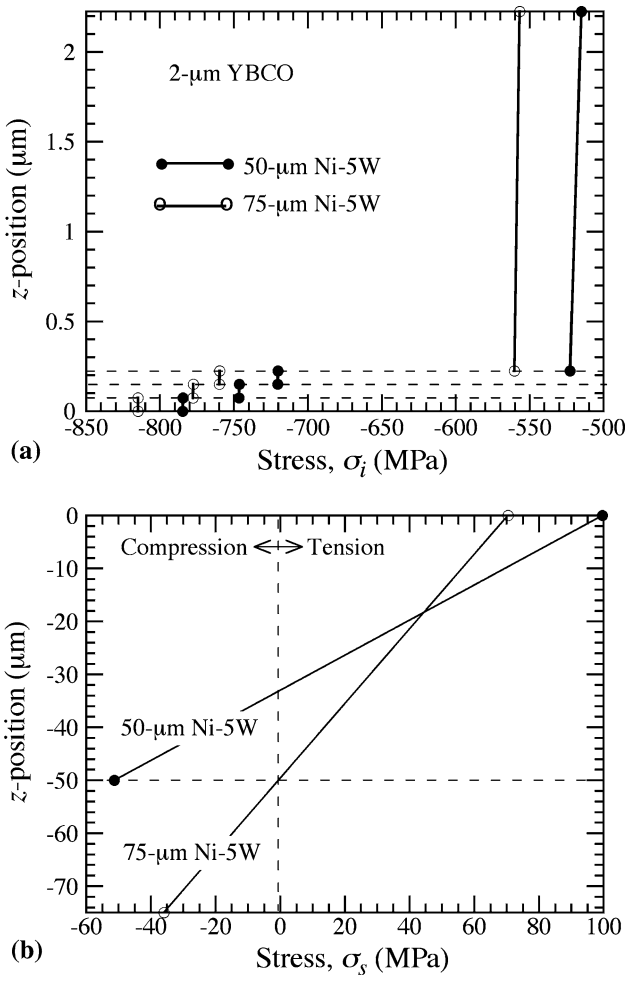

Fig. 6 Thermal stresses in (**a**) YBCO/CeO_2/YSZ/Y_2O_3 films and (**b**) Ni-5 W substrate showing the effects of substrate thickness

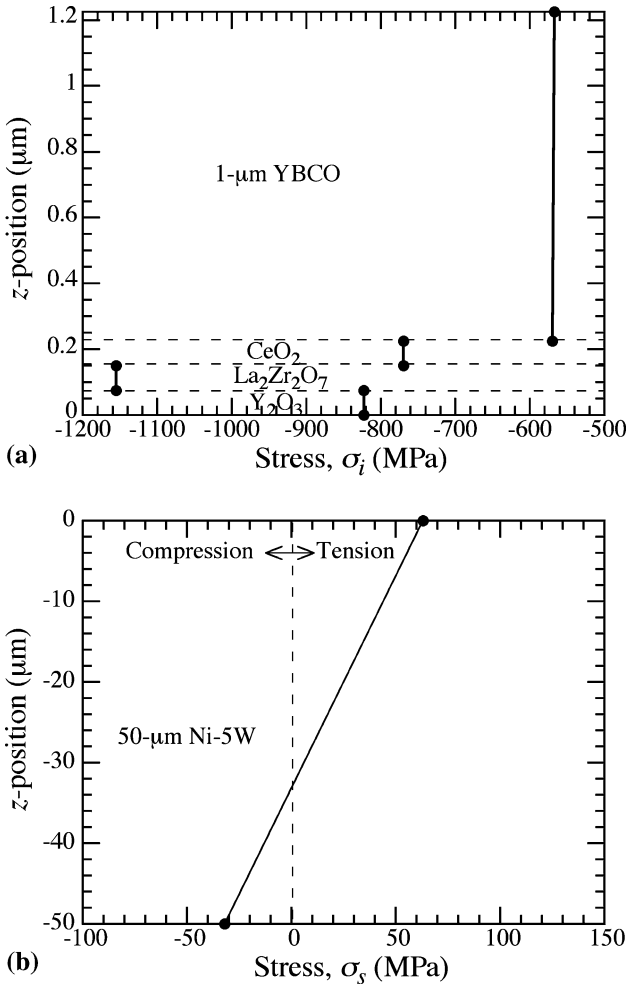

Fig. 7 Thermal stresses in (**a**) YBCO/CeO_2/$La_2Zr_2O_7$/Y_2O_3 films and (**b**) Ni-5 W substrate. The effects of replacing YSZ layer with $La_2Zr_2O_7$ layer can be observed by comparing with Fig. 4a and d

results in a higher residual compressive stress in $La_2Zr_2O_7$ than in YSZ while stresses in other layers remain almost the same. This is because (i) $La_2Zr_2O_7$ has a relatively low CTE and (ii) its thickness (75 nm) is negligible compared to the substrate thickness and its properties change has negligible effects on the stresses in other layers. The curvature change of the system is negligible (from 1.045 to 1.079×10^{-5}/μm) when YSZ layer is replaced by $La_2Zr_2O_7$.

Effects of buffer layers on thermal stresses

The role of buffer layers in thermal stresses in superconductor systems was examined by using 1–3 μm YBCO/30 nm $LaMnO_3$/30 nm homo-epi MgO/10 nm IBAD MgO/7 nm Y_2O_3/80 nm Al_2O_3/50 μm Hastelloy seven-layered IBAD-based superconductor system as an example which is schematically shown in Fig. 8. The thermomechanical properties of the constituent layers are listed in Table 2 (M. Paranthaman, Private communication) [17, 19, 20, 38–41]. Due to the lack of data to differentiate homo epitaxial MgO from IBAD MgO, both were assumed to have the same properties, and $\Delta T = -725$°C was also adopted to calculate thermal stresses.

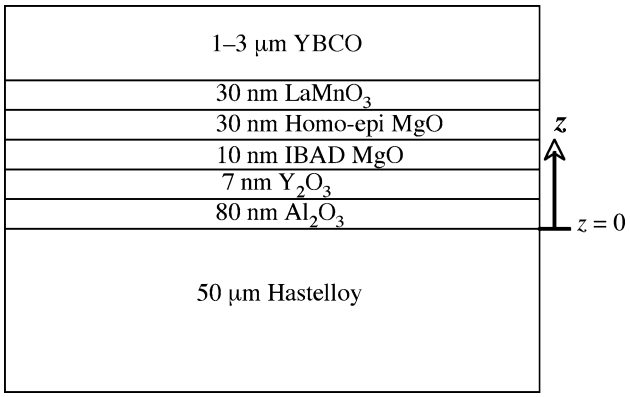

Fig. 8 Schematic showing the layer arrangement and dimensions of the multilayered superconductor system consisting of YBCO/$LaMnO_3$/MgO/MgO/Y_2O_3/Al_2O_3 film layers on Hastelloy substrate

Table 2 Thickness and materials properties of the constituent layers in YBCO/$LaMnO_3$/MgO/MgO/Y_2O_3/Al_2O_3/Hastelloy seven-layered IBAD-based superconductor system

Materials	Thickness	Young's modulus (GPa)	Poisson's ratio	CTE × 10^{-6}/°C
YBCO	1–3 μm	157 [17]	0.3 [17]	12 (M. Paranthaman, Private communication)
$LaMnO_3$	30 nm	178 [38]	0.34 [38]	12 [39]
MgO (homo-epi)	30 nm	162 [40]	0.18 [40]	13 (M. Paranthaman, Private communication)
MgO (IBAD)	10 nm	162 [40]	0.18 [40]	13 (M. Paranthaman, Private communication)
Y_2O_3	7 nm	128 [19]	0.3	9.3 [20]
Al_2O_3	80 nm	174 [41]	0.2 [41]	6.9 [41]
Hastelloy	50 μm	180 [21]	0.33	16 (M. Paranthaman, Private communication)

All the references are given in square brackets

Table 3 Thermal stresses at the upper and lower surfaces and net force per unit width (mm) in each layer for YBCO thickness of 1, 2, and 3 μm

Materials	1 μm YBCO		2 μm YBCO		3 μm YBCO	
	Stress (MPa) Upper Lower	Force mN	Stress (MPa) Upper Lower	Force mN	Stress (MPa) Upper Lower	Force mN
YBCO	–599.41 −600.89	−600.15	−559.14 −564.33	−1123.5	−520.7 −531.51	−1578.3
$LaMnO_3$	−722.56 −722.61	−21.68	−678.59 −678.69	−20.36	−639.13 −639.26	−19.18
MgO (homo-epi)	−386.10 −386.14	−11.58	−353.93 −353.99	−10.62	−325.04 −325.14	−9.75
MgO (IBAD)	−386.14 −386.15	−3.86	−353.99 −354.02	−3.54	−325.14 −325.17	−3.25
Y_2O_3	−1166.1 −1166.1	−8.16	−1136.4 −1136.4	−7.95	−1109.7 −1109.7	−7.77
Al_2O_3	−1008.6 −1008.7	−80.69	−973.21 −973.41	−77.87	−941.46 −941.74	−7.53
Hastelloy	59.06 −30.01	726.12	102.64 −52.89	1243.8	141.76 −74.02	1693.6

The calculated thermal stresses in the seven-layered system are listed in Table 3 for YBCO thicknesses of 1, 2, and 3 μm. The trends of the effects of YBCO thickness on thermal stresses in the seven-layered system are the same as those shown in Fig. 4 for the five-layered system. Since the stresses are linear in each constituent layer, only the stresses at the upper and lower surfaces of each layer are listed. Also, because of the linear stress distribution, the net force per unit width in each layer is the average of the stresses at the upper and lower surfaces multiplied by the layer thickness. The net force per unit (mm) width in each layer is also listed in Table 3. Although the stresses in each buffer layer are quite significant, the net force is relatively small because of the small thickness. To explicitly examine how the presence of buffer layers influences thermal stresses in YBCO, the buffer layers were fictitiously removed from the seven-layered system, such that it became YBCO/Hastelloy bilayer, and the calculated results are listed in Table 4. The differences in the forces between the seven-layered and bilayered systems were also calculated and shown in Table 4. Without the buffer layers, the magnitude of the net force resulting from thermal stresses increases by ~1.4% in YBCO. Hence, the functions of buffer layers are mainly to promote the biaxial texture of YBCO and to serve as diffusion barrier but not to mitigate thermal stresses in YBCO.

Conclusions

Residual stresses resulting from the lattice and the thermal mismatches in the multilayered superconductor system of 1–3 μm YBCO/75 nm CeO_2/75 nm YSZ/75 nm Y_2O_3 films on 50–75 μm Ni-5 W substrates were calculated

Table 4 Thermal stresses at the upper and lower surfaces and net force per unit width (mm) in each layer for YBCO thickness of 1, 2, and 3 μm in the absence of buffer layers

Materials	1 μm YBCO		2 μm YBCO		3 μm YBCO	
	Stress (MPa) Upper Lower	Force mN	Stress (MPa) Upper Lower	Force mN	Stress (MPa) Upper Lower	Force mN
YBCO	−607.93	−608.6	−567.31	−1139.4	−528.52	−1601
	−609.17		−572.05		−538.72	
Difference		1.41%		1.42%		1.44%
Hastelloy	49.42	608.6	93.88	1139.4	133.81	1601
	−25.07		−48.31		−69.78	
Difference		16.2%		8.4%		5.5%

using closed-form solutions. The lattice mismatches between the substrate and films are quite significant, and the predicted residual stresses are too high for the system to withstand. Hence, interfacial defects (e.g., lattice distortion, tilting of the lattice plane, or misfit dislocations/stacking faults) must be formed during the film growth processes to relax lattice mismatch-induced residual stresses. Studies of residual thermal stresses showed the following. When the thickness of a film is negligible compared to the substrate, the changes of its properties modify the residual stresses in this film layer but have negligible effects on the residual stresses in other layers in the system. For example, when 75 nm YSZ in the five-layered system is replaced by $La_2Zr_2O_7$ of the same thickness, the change in residual stress is noticeable only in the $La_2Zr_2O_7$ layer. On the other hand, when the thickness of certain film layer is not negligible compared to the substrate, residual stresses in each layer can be controlled by changing the properties and thickness of this film layer. For example, residual stresses in all constituent layers changes when the thickness of YBCO increases from 1 to 3 μm as shown in Fig. 4. Also, when the films are much thinner than the substrate and the system is subjected to residual stresses, the location of the neutral axis should be located at about two-thirds of the substrate thickness underneath the film/substrate interface. This serves as a checkpoint for the accuracy of results predicted from different models.

The role of buffer layers in thermal stresses in superconductor systems was examined by using YBCO/$LaMnO_3$/homo-epi MgO/IBAD MgO/Y_2O_3/Al_2O_3/Hastelloy seven-layered superconductor system as an example. Although the stresses in each buffer layer are quite significant, the net force in each buffer layer is relatively small because of the small thickness. It is concluded that the functions of buffer layers are mainly to promote the biaxial texture of YBCO and to serve as diffusion barrier but not to mitigate thermal stresses in YBCO.

Since residual stresses can result in cracking and/or delamination, affect the functionality of the film layer, and create a major reliability problem for the applications of multilayered superconductor systems, it is crucial to be able to predict and control these stresses. The closed-form predictive solutions provide guidelines for designing multilayered systems with improved reliability. Depending upon which layer is susceptible to damage in the multilayered system, the corresponding residual stresses should be minimized by judicious choice of layer properties/thicknesses guided by the closed-form solutions. However, it should be noted that the edge effects were not addressed here. When edge delamination is of concern, the dependences of the driving forces for Modes I and II edge delamination for each interface on the material properties and thickness of each layer can be found in a recent publication [42].

Acknowledgements The authors thank Dr. E. D. Specht and Dr. A. Shyam for reviewing the manuscript. This work was jointly sponsored by US Department of Energy, Office of Electricity Delivery and Energy Reliability—Superconductivity for Electric Systems Program and Office of Science, Office of Basic Energy Sciences, Division of Materials Science and Engineering under contract DE-AC05-00OR22725 with UT-Battelle, LLC.

References

1. Paranthaman M, Izumi T (2004) MRS Bull 29:533
2. Paranthaman M, Sathyamurthy S, Heatherly L, Martin PM, Goyal A, Kodenkandath T et al (2006) Physica C 445–448:529. doi:10.1016/j.physc.2006.06.006
3. Goyal A, Paranthaman M, Schoop U (2004) MRS Bull 29:552
4. Stoney GG (1909) Proc R Soc Lond 82:172. doi:10.1098/rspa.1909.0021
5. Timoshenko S (1925) J Opt Soc Am 11:233
6. Saul RH (1969) J Appl Phys 40:3273. doi:10.1063/1.1658174
7. Olsen GH, Ettenberg M (1977) J Appl Phys 48:2543. doi:10.1063/1.323970
8. Feng ZC, Liu HD (1983) J Appl Phys 54:83. doi:10.1063/1.331690

9. Iancu OT, Munz D, Eigenman B, Scholtes B, Macherauch E (1990) J Am Ceram Soc 73:1144. doi:10.1111/j.1151-2916.1990.tb05170.x
10. Liu HC, Murarka SP (1992) J Appl Phys 72:3458. doi:10.1063/1.351420
11. Shaw LL (1998) Compos Part B-Eng 29:199. doi:10.1016/S1359-8368(97)00029-2
12. Hsueh CH (2002) J Appl Phys 91:9652. doi:10.1063/1.1478137
13. Hsueh CH (2002) Thin Solid Films 418:182. doi:10.1016/S0040-6090(02)00699-5
14. Hsueh CH, DeJonghe LC, Lee CS (2006) J Am Ceram Soc 89:251. doi:10.1111/j.1551-2916.2005.00658.x
15. Hu YY, Huang WM (2004) J Appl Phys 96:4154. doi:10.1063/1.1786339
16. Zhang NH, Chen JZ (2008) J Appl Mech 75:044503. doi:10.1115/1.2912994
17. Cheon JH, Shankar PS, Singh JP (2005) Supercond Sci Technol 18:142. doi:10.1088/0953-2048/18/1/022
18. Arda L, Ataoglu S, Sezer S, Abdulaliyev Z (2007) Surf Coat Technol 202:439. doi:10.1016/j.surfcoat.2007.06.008
19. Ochando IM, Cáceres D, García-López J, Escobar-Galindo R, Jiménez-Rioboó RJ, Prieto C (2007) Vacuum 81:1457. doi:10.1016/j.vacuum.2007.04.028
20. Lee CK, Kim WS, Park HH, Jeon H, Pae YH (2005) Thin Solid Films 473:335. doi:10.1016/j.tsf.2004.08.009
21. Clickner CC, Ekin JW, Cheggour N, Thieme CLH, Qiao Y, Xie YY et al (2006) Cryogenics 46:432. doi:10.1016/j.cryogenics.2006.01.014
22. Sanchez-Herencia AJ, Pascual C, He J, Lange FF (1999) J Am Ceram Soc 82:1512
23. Nagai H (1974) J Appl Phys 45:3789. doi:10.1063/1.1663861
24. Ayers JE, Ghandhi SK, Schowalter LJ (1991) J Cryst Growth 113:430. doi:10.1016/0022-0248(91)90077-I
25. Zheleva T, Jagannadham K, Narayan J (1994) J Appl Phys 75:860. doi:10.1063/1.356440
26. Riesz F (1996) J Vac Sci Technol A 14:425. doi:10.1116/1.580100
27. Huang XR, Bai J, Dudley M, Dupuis RD, Chowdhury U (2005) Appl Phys Lett 86:211916. doi:10.1063/1.1940123
28. Cantoni C, Goyal A, Schoop U, Li X, Rupich MW, Thieme C et al (2005) IEEE Trans Appl Supercond 15:2981. doi:10.1109/TASC.2005.848691
29. Qiu Y, Li M, Liu G, Zhang B, Wang Y, Zhao L (2007) J Cryst Growth 308:325. doi:10.1016/j.jcrysgro.2007.08.017
30. Xiong J, Qin W, Cui X, Tao B, Tang J, Li Y (2006) Physica C 442:124. doi:10.1016/j.physc.2006.05.024
31. Chirayil TG, Paranthaman M, Beach DB, Lee DF, Goyal A, Williams RK et al (2000) Physica C 336:63. doi:10.1016/S0921-4534(00)00089-7
32. Bhuiyan MS, Paranthaman M, Salama K (2006) Supercond Sci Technol 19:R1. doi:10.1088/0953-2048/19/2/R01
33. Molina L, Knoth K, Engel S, Holzapfel B, Eibl O (2006) Supercond Sci Technol 19:1200. doi:10.1088/0953-2048/19/11/019
34. Obrador X et al (2006) Supercond Sci Technol 19:S13. doi:10.1088/0953-2048/19/3/003
35. Celik E, Sayman O, Karakuzu R, Ozman Y (2007) Mater Des 28:2184
36. Zhu XB et al (2007) Physica C 467:73. doi:10.1016/j.physc.2007.08.008
37. Knoth K, Hühne R, Oswald S, Schultz L, Holzapfel B (2007) Acta Mater 55:517. doi:10.1016/j.actamat.2006.08.040
38. Darling TW, Migliori A, Moshopoulou EG, Trugman SA, Neumeier JJ, Sarrao JL et al (1998) Phys Rev B 57:5093. doi:10.1103/PhysRevB.57.5093
39. Kartopu G, Es-Souni M (2006) J Appl Phys 99:033501. doi:10.1063/1.2164534
40. Huang QJ, Cheng Y, Liu XJ, Xu XD, Zhang SY (2006) Ultrasonics 44:e1223. doi:10.1016/j.ultras.2006.05.193
41. Thurn J, Cook RF (2004) J Mater Sci 39:4809. doi:10.1023/B:JMSC.0000035319.81486.62
42. Hsueh CH, Luttrell CR, Lee S, Wu TC, Lin HY (2006) J Am Ceram Soc 89:1632. doi:10.1111/j.1551-2916.2006.00924.x